

# Effects of poly(ethylene glycol) on the morphology and properties of biocomposites based on polylactide and cellulose nanofibers

Fatemeh Safdari · Pierre J. Carreau  · Marie C. Heuzey · Musa R. Kamal

Received: 25 December 2016 / Accepted: 5 May 2017 / Published online: 12 May 2017  
© Springer Science+Business Media Dordrecht 2017

**Abstract** Polylactide (PLA)/cellulose nanofiber (CNF) biocomposites were prepared via solution casting and direct melt mixing. To improve the compatibility, a masterbatch of CNFs and poly(ethylene glycol) (PEG) (1:2) was also prepared. The effects of PEG on the morphology and properties of the biocomposites were investigated. The dispersion/distribution of nanofibers in PLA was improved when the masterbatch was used and the composites were prepared in solution. Substantial effects on the rheological properties of solution-prepared PLA/CNF/PEG composites were observed compared to composites containing no PEG, whereas for melt-prepared composites no significant changes were detected. Increased crystalline content and crystallization temperature were observed for the composites prepared via the masterbatch and solvent casting. The storage modulus of PLA was increased by 42 and 553% at 25

and at 80 °C, respectively, for the solution-based PEG-compatibilized composite containing 2 wt% nanofibers. Also, a better light transmittance was measured for the PLA/CNF/PEG composites prepared in solution.

**Keywords** Biocomposites · Polylactide (PLA) · Cellulose nanofibers (CNFs) · Rheology · Crystallinity · Thermomechanical properties · Transparency

## Introduction

Sustainability and environmental considerations have made it desirable to use polymers derived from renewable resources as alternatives to petroleum-based polymers (Raquez et al. 2013). In this regard, bio-derived polylactide (PLA) has been the frontrunner among other biopolymers, owing to its interesting mechanical properties such as high modulus and tensile strength at room temperature (Baiardo et al. 2003), relatively good processability, low toxicity, moderate cost, UV stability, and gloss (Wu 2009; Li et al. 2010; Qu et al. 2010; Siró and Plackett 2010; Tingaut et al. 2010; La Mantia and Morreale 2011; Tome et al. 2011; Adeosun et al. 2012; Marais et al. 2012; Plummer et al. 2013; Raquez et al. 2013; Lu et al. 2014). PLA has found many applications in different fields including biomedical, automotive, electronics, and packaging (Nakagaito et al. 2009;

---

**Electronic supplementary material** The online version of this article (doi:10.1007/s10570-017-1327-5) contains supplementary material, which is available to authorized users.

---

F. Safdari · P. J. Carreau (✉) · M. C. Heuzey  
Chemical Engineering Department, Research Center for High Performance Polymer and Composite Systems (CREPEC), Polytechnique Montreal, Montreal, QC H3C 3A7, Canada  
e-mail: pcarreau@polymtl.ca

M. R. Kamal  
Chemical Engineering Department, CREPEC, McGill University, Montreal, QC H3A 0C5, Canada

Suryanegara et al. 2009; Jonoobi et al. 2010; Sanchez-Garcia and Lagaron 2010; Tingaut et al. 2010; Frone et al. 2011, 2013; Tome et al. 2011; Lee et al. 2012; Marais et al. 2012; Wang and Drzal 2012; Zhou et al. 2013). However, the use of PLA for many applications presents a variety of issues, e.g. slow crystallization (Suryanegara et al. 2009) and low heat resistance (low stiffness at elevated temperatures) (Suryanegara et al. 2009; Qu et al. 2010; Siró and Plackett 2010; Adeosun et al. 2012; Abdulkhani et al. 2014; Lu et al. 2014). One of the promising approaches that can circumvent these limitations is the use of reinforcements (Siró and Plackett 2010; Abdulkhani et al. 2014). It is important that the advantages of PLA such as biocompatibility, biodegradability and transparency can be maintained when choosing an appropriate reinforcement. To this end, some common nanofillers (e.g. carbon nanotubes) may not be appropriate as they are not biocompatible and biodegradable and that they may deteriorate the transparency of the matrix.

Cellulose nanofibers (CNFs) have shown excellent properties of interest as reinforcement in composites, including high sound attenuation, high strength and modulus, large aspect ratio and surface area, biodegradability, biocompatibility, low density, low cost, nontoxicity and non-abrasiveness to the processing equipment (Azizi Samir et al. 2005; Petersson and Oksman 2006; Brown and Laborie 2007; Wang and Sain 2007; Iwatake et al. 2008; Nakagaito et al. 2009; Suryanegara et al. 2009; Wu 2009; Eichhorn et al. 2010; Jonoobi et al. 2010; Qu et al. 2010; Sanchez-Garcia and Lagaron 2010; Tingaut et al. 2010; Kowalczyk et al. 2011; Adeosun et al. 2012; Jonoobi et al. 2012; Lee et al. 2012; Wang and Drzal 2012; Frone et al. 2013; Plummer et al. 2013; Raquez et al. 2013; Abdulkhani et al. 2014; Lu et al. 2014; Xu et al. 2014; Tercjak et al. 2015). Thus, the use of CNFs to develop reinforced PLA composites, considering their entirely bio-based nature, would be preferable over that of inorganic particles (Iwatake et al. 2008; Suryanegara et al. 2009; Kowalczyk et al. 2011).

Achieving uniformly dispersed nanofibers in PLA and assuring nanofiber–polymer interfacial compatibility are important challenges in the preparation of PLA/CNF biocomposites. This is due to the very strong hydrogen bond interactions between the long and flexible CNFs that cause their agglomeration. Furthermore, the difference in polarity between PLA and CNFs favors agglomeration (Tome et al. 2011;

Jonoobi et al. 2012; Plummer et al. 2013; Safdari et al. 2016b). Therefore, special processing methods and compatibilization strategies are required to promote interfacial compatibility. Good dispersion with minor agglomeration of CNFs may be obtained by compatibilization through chemical modification of either nanofibers (Wang and Sain 2007; Lee et al. 2009; Li et al. 2010; Tingaut et al. 2010; Frone et al. 2011, 2013; Tome et al. 2011; Jonoobi et al. 2012; Plummer et al. 2013; Abdulkhani et al. 2014; Lu et al. 2014) or PLA (Marais et al. 2012; Lu et al. 2014). The use of a compatibilizer as a third component, which may be easier and more cost effective, can be an interesting alternative (Mathew et al. 2006; Wang and Sain 2007; Qu et al. 2010; Lee et al. 2012). In most cases, compatibilization is conducted in solution and a drying step is needed prior to the addition of compatibilized CNFs to the matrix. However, the tendency to agglomerate during the drying step would make re-dispersion of compatibilized CNFs in the matrix in molten state still difficult. Thus, composite preparation in solution could be a good alternative to achieve good dispersion (Iwatake et al. 2008; Suryanegara et al. 2009; Jonoobi et al. 2010; Kowalczyk et al. 2011).

Several efforts have been made to produce PLA/CNF biocomposites with nanofiber contents of 1–5 wt% and using a compatibilizer to enhance the properties of PLA, but with limited success so far. Mathew et al. (2006) prepared cellulose microfibril (CMF)-reinforced PLA by adding poly(ethylene glycol) (PEG) as a processing aid. However, the tensile strength remained unchanged and the Young modulus increased by only 15% for the compatibilized PLA/CMF composite containing 5 wt% fibers and 5 wt% PEG compared to PLA. Wang and Sain (2007) modified hemp nanofibers (HPNs) using styrene maleic anhydride copolymer (SMA) in solution. The dispersion of the modified nanofibers in PLA was not uniform and agglomerates were still formed. The tensile strength and Young modulus increased by 9 and 10%, respectively, for the composite sample containing 5 wt% SMA-modified HPNs. Qu et al. (2010) also prepared PLA/CNF composites using PEG as the compatibilizer in a solvent-casting method with CNF/PEG at a ratio 3/2. The tensile strength was slightly increased from ca. 40 MPa for PLA to ca. 45 MPa for the PLA/CNF/PEG sample containing 2 wt% fibers. Lee et al. (2012) incorporated bio-

derived polylactide carbohydrate copolymer to compatibilize bacterial cellulose nanofibers (BCNFs) with PLA. Both the glass transition and crystallization temperatures of the matrix were reduced for the composite containing 5 wt% BCNFs with 4.75 wt% copolymer, while the crystalline content of PLA increased. The tensile strength and Young modulus of the composite were improved by 7 and 15%, respectively, compared to PLA.

In our previous work (Safdari et al. 2016a, b), CNFs were incorporated into PLA via solvent casting to overcome some of its drawbacks, e.g. slow crystallization and low heat resistance, which could successfully improve the properties in different aspects without deteriorating the thermal stability and transparency of the matrix. In the current study, in order to further improve the dispersion/distribution of nanofibers within the PLA matrix, PEG is used as a compatibilizer to produce biocompatible and biodegradable PLA/CNF/PEG composites. The choice of PEG is justified by its miscibility with PLA (Sheth et al. 1997; Baiardo et al. 2003; Buddhiranon et al. 2011; Arias et al. 2015) and its better affinity with CNFs compared to PLA. A solvent-casting technique is used to prepare PLA/CNF/PEG composites with enhanced properties at low nanofiber loadings. Effects of PEG on the morphological, rheological, thermal, mechanical, and optical properties of the CNF-reinforced PLA composites are then reported. This work shows that the rheological properties are correlated with the quality of the dispersion/distribution of CNFs in the matrix and the thermomechanical properties of the polymer/CNF composites. To our knowledge, such full characterization of PLA/CNF composites with the emphasis on the improved CNF dispersion/distribution that could successfully lead to major property enhancements has not been reported.

## Experimental section

### Materials

A polylactide (PLA) (Ingeo Biopolymer 3251D, NatureWorks, Minnetonka, MN, USA) with a melting point of 155–170 °C, weight-average molecular weight of 55,000 g/mol, and polydispersity index of 1.62 (Zhang et al. 2014) was used. A poly(ethylene

glycol) (PEG) in flake form with a number-average molecular weight of 20,000 g/mol and a melting point of 63–66 °C was purchased from Sigma-Aldrich Canada Co. (Oakville, ON, Canada). The solvent, *N,N*-dimethylformamide (DMF), was used as received (anhydrous 99.8% from Sigma-Aldrich Canada Co., Oakville, ON, Canada). An aqueous suspension containing 2.3 wt% cellulose nanofibers (CNFs), with a diameter less than 50 nm and length of several micrometers, was kindly provided by Prof. Mohini M. Sain following the methodology described in Janardhnan and Sain (2011). A copper(II)-ethylene-diamine complex 1.0 M in H<sub>2</sub>O (Sigma-Aldrich Canada Co., Oakville, ON, Canada) was used to stain the CNFs in composites prior to the transmission electron microscopy.

### Sample preparation

The aqueous suspension of CNFs was freeze-dried for 48 h (Labconco Freezone 2.5<sup>Plus</sup>). The freeze-dried CNFs were mixed with an appropriate amount of DMF in an Erlenmeyer to form CNF suspensions containing 4–10 g of CNFs per L of DMF. The suspension was sonicated for 1 h using a water-bath sonicator (FS30 100 Watts Ultrasonic Cleaner, Fisher Scientific, Pittsburgh, PA, USA) and, then, stirred for 1 more hour using a magnetic stirrer at 400 rpm. Vacuum-dried PLA, at 80 °C for 24 h, was added to the suspension and stirred at 400 rpm, 70 °C and for 2 h until the PLA pellets were completely dissolved. Finally, the mixture was vacuum dried in an oven at 80 °C for 24 h, and, the product was then ground into small granules using a laboratory grinder (Janke & Kunkel A10S1 model, IKA WERK, Germany) and kept again for 48 h in a vacuum oven at 60 °C.

A masterbatch of CNFs and PEG was prepared via an aqueous mixing method at ambient temperature. The original CNF aqueous suspension was diluted with distilled water in an Erlenmeyer using a magnetic stirrer at 400 rpm for 1 h to form a 1 wt% CNF suspension and the desired amount of PEG was added for a weight ratio of CNFs to PEG 1:2, then, stirred for 1 more hour. Finally, the mixture was vacuum dried for 48 h at 50 °C to be used as the masterbatch of compatibilized CNFs for the composite fabrication following the same solution-preparation technique described above. The various samples containing CNFs or PEG or CNF/PEG masterbatch are identified

based on their fiber and PEG contents, 0–5 and 0–4 wt%, respectively. For instance, PLA/2CNF/4PEG denotes composite containing 2 wt% CNFs and 4 wt% PEG of the overall composite. The samples of the neat PLA and PLA/4PEG were also produced using a similar procedure to compare the results.

To investigate the effect of different preparation techniques on the dispersion and distribution of nanofibers and final properties of the biocomposites, the neat PLA and biocomposites were also prepared in the melt using an internal mixer, DDRV501 Brabender (C. W. Brabender Instruments Inc., NJ, USA). These samples are denoted with a “(M)”, referring to preparation in the molten state. For this purpose, the as-received PLA and PEG were dried at 80 and 50 °C, respectively, under vacuum for 24 h. The freeze-dried CNFs, the masterbatch or PEG were directly melt-compounded with PLA for 7 min, at 100 rpm and 180 °C under nitrogen. Thereafter, the samples were immersed in liquid nitrogen, then ground into small granules.

Finally, all the samples formulated using both methods, solution and melt, were molded using a compression press (12 Ton Manual Hydraulic Press, Carver, Inc., Wabash, IN, USA) at 175 °C for 10 min in the presence of nitrogen to prepare different test specimens. The pressure was gradually increased up to 29 kPa. After compression molding, the samples were cooled in the press under 29 kPa at room temperature for 5 min and, then, were kept under vacuum before subsequent testing.

## Characterization

### Microscopy

Gold-coated microtomed sample surfaces were investigated by scanning electron microscopy (SEM) using a JSM 7600TFE microscope (JEOL USA, Inc., Peabody, MA, USA).

For transmission electron microscopy (TEM), the samples were microtomed at ca.  $-100$  °C with a diamond knife into slices with an approximate thickness of 50–80 nm using an Ultracut FC microtome (Leica Biosystems Inc., Concord, ON, Canada). Then, the ultra-microtomed sample slices were characterized by TEM using a JEM 2100F microscope (JEOL USA, Inc., Peabody, MA, USA). For a better visualization of nanofibers, the samples were stained using a

copper(II)-ethylenediamine complex 1.0 M in H<sub>2</sub>O. The details of the staining are given elsewhere (Bagheriasl et al. 2016b).

Images of ultra-microtomed surfaces of composites were obtained using a multimode scanning probe in tapping mode on Dimension FastScan atomic force microscope (AFM) with ScanAsyst<sup>TM</sup> from BRUKER (Billerica, MA, USA).

### Rheology

The rheological properties were measured at 175 °C in the presence of nitrogen using a stress-controlled rheometer (MCR 301, Anton Paar, Austria). A cone-and-plate geometry with 0.051 mm cone truncation, ca. 2° cone angle and 25 mm diameter, was used to perform the measurements in small-amplitude oscillatory shear (SAOS) mode in the linear viscoelastic region. The thermal stability in time sweep tests was assessed at 1 rad/s frequency for 15 min. All the samples exhibited stable rheological properties, with changes less than 4%, in time-sweep tests. A strain amplitude of 0.05 was used to perform frequency sweeps within the time limit of measurements (i.e., 15 min).

### Mechanical and thermal properties

For thermogravimetric analysis (TGA), a TGA Q500 (TA Instruments, New Castle, DE, USA) was used in high-resolution mode. The samples were heated to 800 °C at a rate of 10 °C/min and a nitrogen flow rate of 60 mL/min. The tests were performed twice on typically 15 mg specimens for each sample.

Differential scanning calorimetry (DSC) was performed using a DSC Q1000 (TA Instruments, New Castle, DE, USA), under nitrogen. A rate of 2 °C/min was chosen to heat the samples, from room temperature to 200 °C, and then, the samples were held at 200 °C for 3 min, and finally cooled (2 °C/min) to 20 °C. Two replicates were tested for each sample.

Tensile tests were performed on specimens with dumb-bell shape type V (standard ASTM D638) using an Instron 3365 (Instron, Norwood, MA, USA). The tests were carried out at room temperature with a load cell of 5 kN and a crosshead speed of 5 mm/min. At least seven specimens per sample were tested.

Dynamic mechanical thermal analysis (DMTA) was performed in flexion mode using a DMA 2980

analyzer (TA Instruments, New Castle, DE, USA). The frequency, amplitude and heating rate were 1 Hz, 30  $\mu\text{m}$  and 2  $^{\circ}\text{C}/\text{min}$  (from room temperature to 120  $^{\circ}\text{C}$ ), respectively. At least three replicates per sample were tested.

### Optical properties

The optical transparency was investigated on films of  $102 \pm 6 \mu\text{m}$  thickness, using a LAMBDA 1050 UV/Vis/NIR Spectrophotometer (PerkinElmer, Waltham, MA, USA). The wavelength range was 250–800 with 5 nm spectral bandwidth and 141 nm/min scanning rate. The test was performed three times for each sample.

## Results and discussion

### SEM

Figure 1 illustrates SEM images of the freeze-dried CNFs (from an aqueous suspension containing 0.1 wt% nanofibers) and PLA containing 2 wt% CNFs with and without PEG. A web-like structure of individual nanofibers and bundles are observed in Fig. 1a–c, even when the nanofibers are dispersed in the preferred medium, i.e., water (Eichhorn et al. 2010). The SEM images of PLA/2CNF, presented in Fig. 1d–f, show a moderately fair dispersion and uniform distribution of the fibers in PLA at the micro level. However, Fig. 1g–i show that CNFs are very well dispersed/distributed within the matrix for the PLA/2CNF/4PEG composite, which is related to the efficient compatibilization effect of PEG; in fact, PEG prevents the intermolecular interactions (hydrogen bonding between the nanofibers) and the agglomeration of the nanofibers by introducing new hydrogen bonding with CNFs (Qu et al. 2010). Also, there is no fiber pull-out for this composite, contrary to the PLA/2CNF sample, suggesting a better adhesion between CNFs and PLA in the presence of PEG.

It is worthwhile to mention that large CNF agglomerates in the melt-prepared composites, i.e., PLA/2CNF (M) and PLA/2CNF/4PEG (M), were observed via naked eye sample visualization (see Fig. S1 in the Supplementary Information). Hence, we did not further investigate the morphology of these two composites.

### TEM

Figure 2a shows the web-like structure of single CNFs and bundles of nanofibers after water evaporation (CNF concentration of 0.5 wt% in the aqueous suspension). TEM images of PLA/2CNF and PLA/2CNF/4PEG are presented in Fig. 2b–e and f–i, respectively. The quality of the nanofiber dispersion/distribution for composites prepared without PEG is clearly different from that for PEG-compatible composites (Fig. 2b–e compared to Fig. 2f–i). For PLA/2CNF in Fig. 2b–e, no large agglomerates are seen, but there are not many single fibers; however, for PLA/2CNF/4PEG in Fig. 2f–i, more CNFs are dispersed individually and/or in the form of bundles with few fibers. Also, the CNF distribution at the nano level is quite good for the sample containing PEG over the other composites. This is a consequence of using the CNF/PEG masterbatch to produce the PLA/2CNF/4PEG sample.

### AFM

AFM analysis was used to provide more insights on the phase morphology, i.e., miscibility/immiscibility of PEG with PLA, and on the dispersion/distribution of nanofibers within PLA. This technique is advantageous to distinguish any phase structures in polymer blends, which may not be easily visualized by other microscopic techniques such as SEM and TEM due to the insufficient contrast, low content of a component, or very fine droplet formation. In fact, the main reason that makes the AFM superior is the capability of characterizing the heterogeneity in a target surface and detecting different components by differences in their polarity and elasticity (Saffar et al. 2016) via adhesion and modulus imaging, respectively. Besides, the topography of the surface can be well determined by height imaging. Considering all the three imaging modes, i.e., height, adhesion, and modulus, one can conclude if the contrast observed in the adhesion or modulus images is caused by topographic variations in the surface or is indicative of different components.

Figures 3a and b present AFM images for the 2 wt% nanofiber composite without PEG and AFM images for the PEG-compatible composite are presented in Fig. 3c–h. PEG and CNFs are both hydrophilic and, therefore, appear similar in adhesion imaging. On the other hand, PEG has a much lower



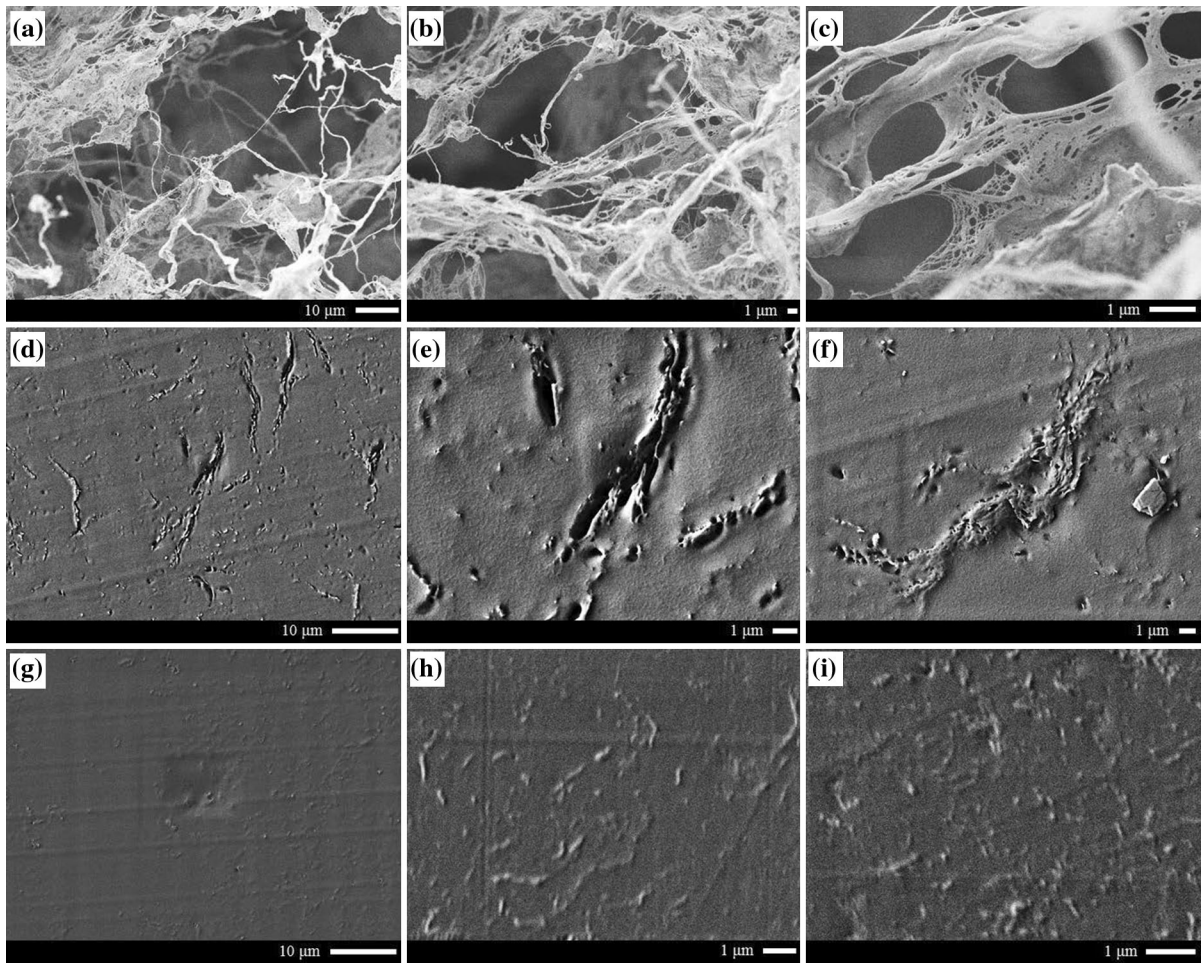
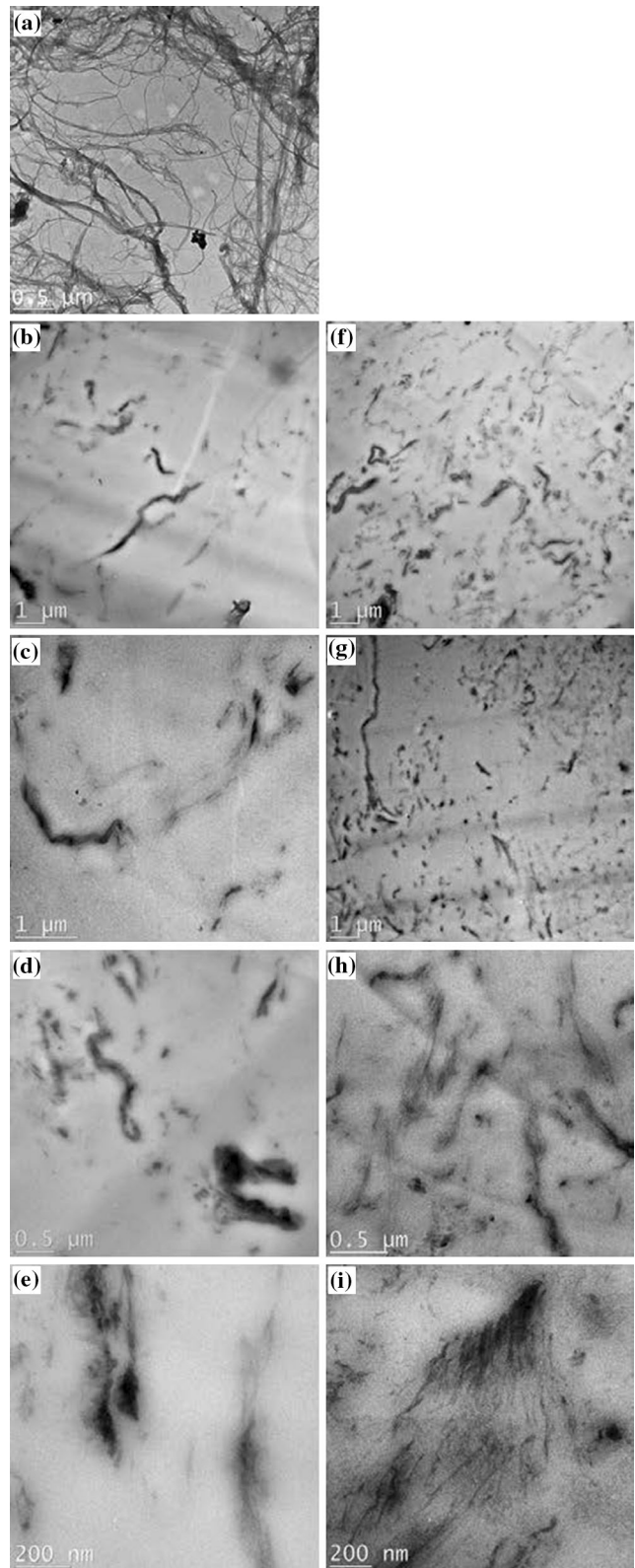


**Fig. 1** SEM images of **a–c** freeze-dried CNFs, **d–f** PLA/2CNF and **g–i** PLA/2CNF/4PEG, taken from different samples and/or at different magnifications

modulus and CNFs have a significantly larger modulus, compared to PLA. Hence, positive height, negative adhesion, and positive modulus indicate the presence of nanofibers, whereas negative adhesion and modulus represent the presence of PEG rich-domains in the sample, if existing. As both height and adhesion (and modulus, if applicable) imaging show clearly, the distribution for the composite without PEG (Fig. 3a, b) is not as uniform as that for PLA/2CNF/4PEG (Fig. 3c–e). The CNFs for the sample prepared using the masterbatch are well distributed throughout the matrix (Fig. 3c–e); also the presence of fibers with a diameter of few nanometers is evident in Fig. 3f–h, revealing the good dispersion of the CNFs. Hence, the AFM analysis confirms that a better dispersion and distribution of CNFs may be achieved when they are

first dispersed in PEG. Moreover, the AFM images of PLA/2CNF/4PEG composite obtained from either adhesion (Fig. 3d, g) or modulus (Fig. 3e, h) imaging do not show a two-phase system, i.e., no dark droplets are observed, indicating that PEG is miscible with PLA for the selected molecular weight and concentration; hence, the nanofibers are distributed over the whole sample. The miscibility of PEG and PLA has been discussed in other investigations from a thermodynamic point of view (Adamska et al. 2016); the two polymers have close values for the solubility parameter and are considered as a miscible polymer pair. However, the PEG molecular weight and its concentration in the PLA matrix have been shown to affect the miscibility range of PEG in PLA, as discussed in by Sheth et al. (1997), Baiardo et al. (2003), and

**Fig. 2** TEM images of **a** dried CNFs (from an aqueous suspension containing 0.5 wt% fibers), **b–e** PLA/2CNF and **f–i** PLA/2CNF/4PEG, taken from different samples and/or at different magnifications





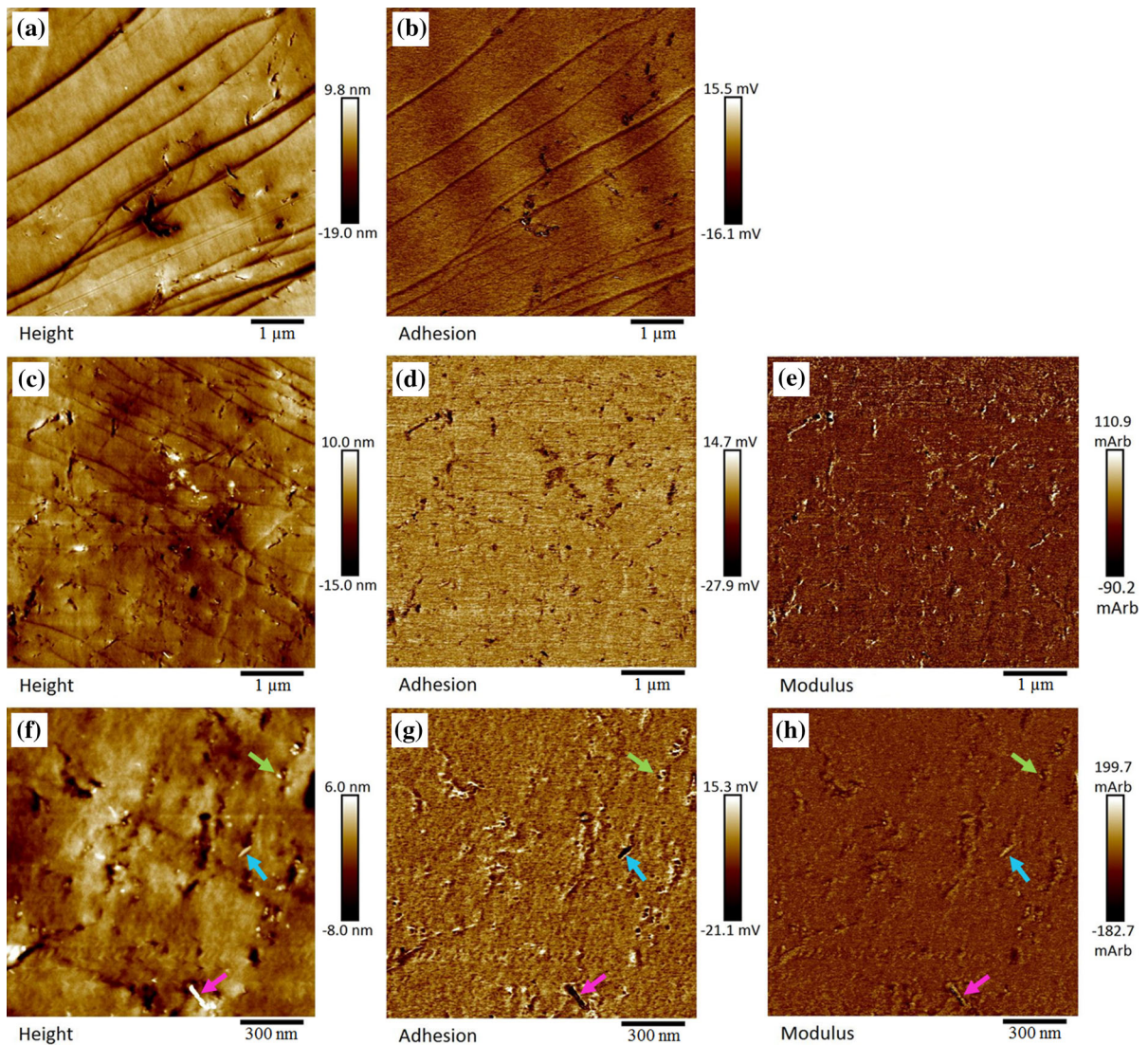


**Fig. 3** AFM images of **a, b** PLA/2CNF and **c–h** PLA/2CNF/4PEG, at different magnifications and for different imaging of height, adhesion and modulus. The *arrows* in **f–h** indicate how a

nanofiber or fiber bundle appears in different imaging. Note that the long parallel lines (especially in **a, b**) are the traces created by the diamond knife during surface preparation

Buddhiranon et al. (2011). Thus, the presence of PEG, being miscible with PLA, is believed to enhance the compatibility of PLA and dispersed CNFs via increased hydrophilicity of the matrix (Hendrick and Frey 2014).

### Rheology

Figure 4 presents SAOS data in terms of the complex viscosity,  $\eta^*$ , and storage and loss moduli,  $G'$  and  $G''$ , as functions of frequency,  $\omega$ , for all solution-produced

samples. PLA exhibits a long plateau for  $\eta^*$  followed by shear thinning (Fig. 4a). Also terminal zones with slopes of two and one are observed for  $G'$  and  $G''$  versus  $\omega$ , respectively (Fig. 4b). All composites show a shear-thinning behavior without a plateau region for  $\eta^*$  (Fig. 4a) and a less frequency-dependency behavior for  $G'$  and  $G''$  (Fig. 4b), especially at lower frequencies. Large increases in  $\eta^*$ ,  $G'$  and  $G''$  by one, four and one orders of magnitude, respectively, are observed for PLA/2CNF relative to the neat PLA (extrapolating the PLA  $G'$  data at low frequencies). The results



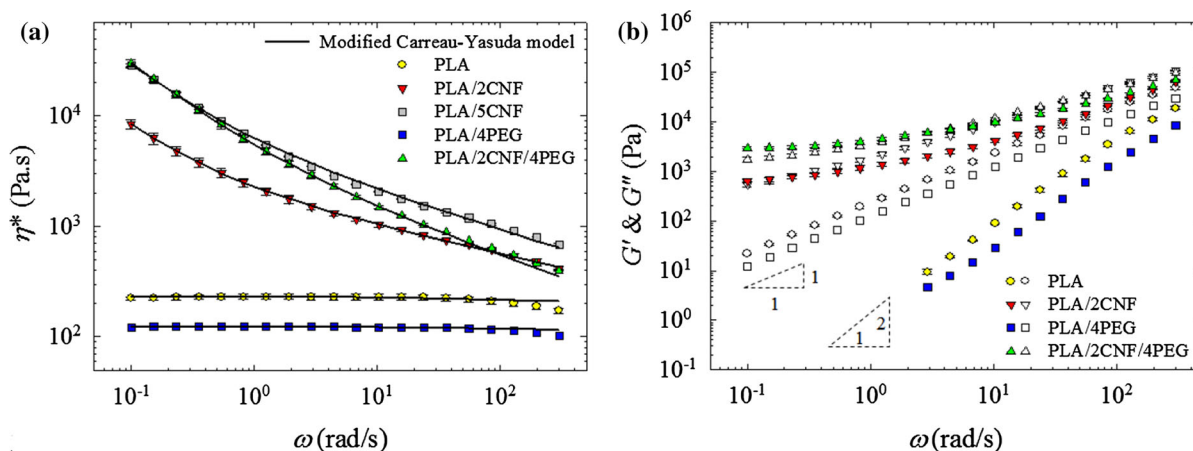


**Fig. 4** **a** Complex viscosity, and **b** storage and loss moduli (*filled* and *open* symbols, respectively) versus frequency at 175 °C and 0.05 strain amplitude for all solution-based samples. The *solid lines* in **a** represent the modified Carreau–Yasuda model fits, Eq. (1)

suggest a network formation, which consequently leads to a transition from liquid- to viscoelastic solid-like behavior, with an upturn in viscosity and plateaus in  $G'$  and  $G''$  at low frequencies. On the other hand, by introducing the masterbatch into PLA, i.e., PLA/2CNF/4PEG sample, the values for  $\eta^*$ ,  $G'$  and  $G''$  of PLA/4PEG at low frequencies increase by two, six and two orders of magnitude (extrapolating the PLA/4PEG  $G'$  data), respectively. Also, Fig. 4b shows that  $G'$  and  $G''$  for PLA/2CNF/4PEG cross over at a frequency higher than that for PLA/2CNF. Interestingly, PLA/2CNF/4PEG exhibits a similar low-frequency complex viscosity behavior as the composite containing more CNFs, but without PEG, i.e., PLA/5CNF (Fig. 4a). In contrast,  $\eta^*$  of PLA/4PEG is lower than that of PLA due to the lower complex viscosity of PEG compared to PLA. In fact, PEG has a Newtonian behavior in the whole range of frequency tested, with a very low value of  $\eta^*$ , ca. 20 Pa.s at 75 °C (already lower than that of PLA at 175 °C), so that it was not feasible to measure its rheological properties at 175 °C for the sake of comparison.

These are indications of a more viscoelastic solid-like behavior in the composite with PEG compared to PLA/2CNF, as a result of stronger CNF–CNF and/or polymer–CNF interactions and, consequently, more restriction to PLA chain mobility. In fact, for the compatibilized composite, in addition to the interfacial interactions through molecular entanglement and mechanical interlocking between CNFs and the polymer matrix (Miao and Hamad 2013), the

nanofibers can have possible electrostatic attractions (hydrogen bonding) with PEG (Brown and Laborie 2007; Qu et al. 2010). However, in some investigations it has been proposed that CNFs may have electrostatic attractions with PLA as well (Frone et al. 2011; Qu et al. 2010), but this is more probable with PEG. Moreover, the better dispersion/distribution of nanofibers in the matrix using the masterbatch method could make a stronger CNF network, as strong as the network that is made in the presence of larger content of nanofibers, i.e., 5 wt%. Therefore, the rheological results (Fig. 4) confirm the SEM, TEM and AFM observations of Figs. 1, 2 and 3. It is worth mentioning that the composite containing 5 wt% CNFs prepared via solution mixing and masterbatch had a complex viscosity,  $\eta^*$ , larger than that of the uncompatibilized PLA/5CNF composite at low frequencies (see Fig. S2 in the Supplementary Information). Composites containing other particles such as cellulose nanocrystals (Khoshkava and Kamal 2014; Kamal and Khoshkava 2015; Bagheriasl et al. 2016a, b), organoclays (Ghanbari et al. 2013a, b) and carbon nanotubes (Abbasi et al. 2009) also showed similar rheological behavior.

If no apparent yield stress is observed as expected for PLA and PLA/4PEG in Fig. 4a, the composites obviously show an apparent yield stress that can be quantified according using the modified Carreau–Yasuda model (Kamal and Khoshkava 2015; Safdari et al. 2016b):

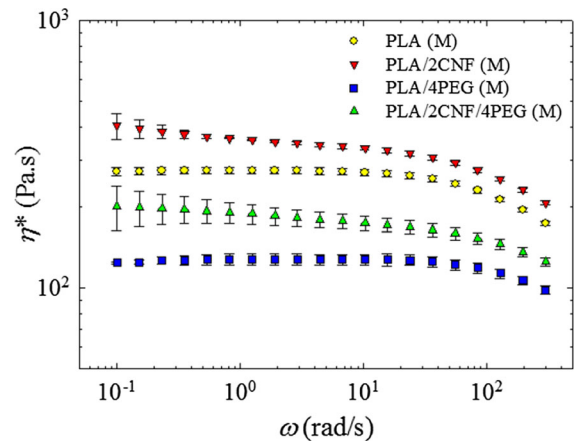
$$\eta^* = \sigma_y/\omega + \eta_0(1 + (\lambda\omega)^a)^{(n-1/a)} \quad (1)$$

**Table 1** Modified Carreau–Yasuda model parameters, Eq. (1)

Sample	$n$	$\sigma_y$ (Pa)	$\lambda$ (s)	$\eta_0$ (Pa s)	$a$
PLA	0.97	0.00	0.100	232	0.99
PLA/2CNF	0.75	531	777	9170	0.87
PLA/5CNF	0.66	1990	963	43,600	0.78
PLA/4PEG	0.98	0.00	0.100	124	0.99
PLA/2CNF/4PEG	0.61	2250	1230	53,500	0.66

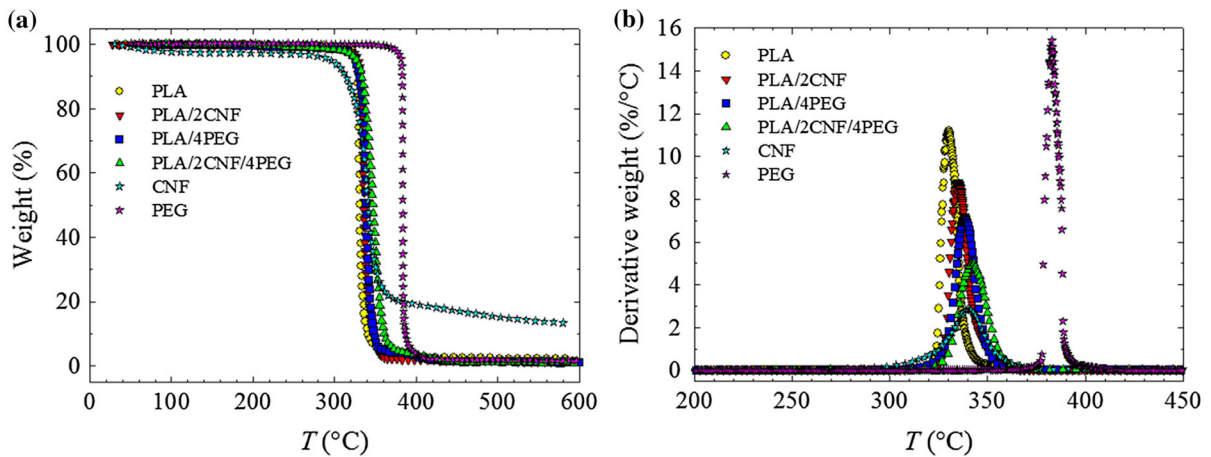
where  $\sigma_y$ ,  $a$ ,  $\lambda$ ,  $n$  and  $\eta_0$  are the apparent yield stress, Yasuda parameter, time constant, flow index and zero-shear viscosity, respectively. Figure 4a shows that the model fits all the composite data very well. The parameters of the model are listed in Table 1. Since this is a 5-parameter (empirical) model, justifying the variations of the parameters with the CNF content is not easy. As the CNF content increases and/or a better CNF dispersion/distribution is achieved  $\sigma_y$  increases, while  $n$  decreases. Also,  $\eta_0$  and  $\lambda$  increase significantly by incorporating the nanofibers. The changes are more significant when the PEG-compatible CNFs is incorporated into the matrix. Therefore, the rheological percolation for PLA/CNF/PEG system might occur at a lower CNF content than that for the system without PEG; however, the determination of a precise percolation threshold for the PLA/CNF/PEG system requires further investigations for composites containing less CNFs. A percolation threshold of 0.5–1 and 1–2 wt% CNFs has been already reported in our previous investigations focused on PLA/CNF (Safdari et al. 2016a, b) and poly(ethylene oxide)/CNF (Safdari et al. 2016c) systems, respectively.

Figure 5 presents  $\eta^*$  as a function of  $\omega$ , for the samples prepared in the melt. Contrary to the results achieved for the samples prepared in solution, the complex viscosity of PLA/2CNF (M) does not increase much relative to the PLA (M). Also, using the CNF/PEG masterbatch does not lead to better results than direct melt mixing of PLA and CNFs. This confirms that because of the long length and high flexibility of the nanofibers that make a highly entangled structure, the CNF dispersion in a matrix remains challenging when a melt mixing step is used. This suggests that the solution preparation method is an effective method to disperse/distribute the fibers within the matrix. Therefore, further measurements in this investigation are mainly reported for solution-based samples.

**Fig. 5** Complex viscosity versus frequency at 175 °C and 0.05 strain amplitude for the samples prepared in the melt

### TGA

Figure 6 presents the thermal degradation behavior in terms of TGA and derivative TGA (DTG) data of the samples prepared in solution. The temperature at which the sample loses 5% of its weight after evaporation of the absorbed moisture occurs at 306, 327 and 380 °C for CNFs, PLA and PEG, respectively (Fig. 6a). All samples, i.e., PLA/2CNF, PLA/4PEG and PLA/2CNF/4PEG, exhibit almost similar values relative to the neat PLA (with differences of 1 °C). DTG data are plotted in Fig. 6b. The onset temperature of degradation occurs at 317 °C for CNFs and at 324 and 378 °C for PLA and PEG, respectively. This occurs at ca. 329 °C for other PLA samples containing either CNFs, PEG or masterbatch. However, the DTG peak temperature for PLA/2CNF, PLA/4PEG and PLA/2CNF/4PEG increases to 334, 338 and 342 °C, respectively, compared to that of PLA (330 °C); for CNFs this temperature appears at 340 °C. The presence of PEG with a higher peak degradation temperature, i.e., 383 °C, increases the peak degradation temperature of PLA. Moreover, the dispersed/distributed nanofibers raise the peak temperature of PLA due to suppression of the polymer chain motion (Ramezani Kakroodi et al. 2014; Ambrosio-Martín et al. 2015; Safdari et al. 2016b, c). Thus, when PEG-compatible CNFs are used to prepare the composite, this temperature shifts to a higher temperature affected by both components, i.e., PEG and CNFs.



**Fig. 6** **a** TGA and **b** DTG plots of samples prepared in solution

## DSC

Table 2 reports cold crystallization ( $T_{cc}$ ), crystallization ( $T_c$ ), and melting ( $T_m$ ) temperatures as well as crystalline contents upon the first heating and first cooling sequences ( $X_c^{heating}$  and  $X_c^{cooling}$ ) of DSC measurements for PEG and samples prepared in solution. The  $X_c^{heating}$  and  $X_c^{cooling}$  values are reported based on the following equations (Ghanbari et al. 2013b)

$$X_c^{heating} = (\Delta H_m - \Delta H_{cc}) \times 100 / (w_m \Delta H_m^0) \quad (2)$$

$$X_c^{cooling} = \Delta H_c \times 100 / (w_m \Delta H_m^0) \quad (3)$$

where the enthalpies of cold crystallization, melting and crystallization are  $\Delta H_{cc}$ ,  $\Delta H_m$  and  $\Delta H_c$ , respectively; the melting enthalpy of 100% crystalline PLA ( $\Delta H_m^0$ ) is 93 J/g (Ambrosio-Martín et al. 2015), and  $w_m$

is the PLA weight fraction. To calculate crystalline contents for PEG sample,  $\Delta H_{cc}$  is zero and  $\Delta H_m^0$  is equal to 201.2 J/g (Brown and Laborie 2007);  $w_m$  refers to the PEG weight fraction and is equal to 1.

Table 2 shows that  $X_c^{heating}$  of PLA is not affected by the addition of 2 wt% CNFs. The crystalline content increases when PEG is added to PLA, this is mostly due to the plasticization role of PEG that increases the polymer chain mobility. However, PLA/2CNF/4PEG exhibits a lower crystallinity than PLA/4PEG due to the restriction of the polymer chain mobility caused by the nanofibers that disrupt the crystalline growth.  $X_c^{cooling}$  of PLA increases up to 33% by adding 2 wt% CNFs and 4 wt% PEG for PLA/2CNF/4PEG. Moreover,  $T_c$  is shifted to higher temperatures for both PLA/2CNF and PLA/2CNF/4PEG samples relative to that of PLA, up to 19 °C for the latter case. This is due to a synergistic effect of PEG

**Table 2** DSC results of PEG and solution-prepared samples for first heating and cooling sequences

Sample	$T_g$ (°C) <sup>a</sup>	$T_{cc}$ (°C)	$T_c$ (°C)	$T_m$ (°C)	$X_c^{heating}$ (%)	$X_c^{cooling}$ (%)
PEG	N/A	N/A	48.4 ± 0.1	65.3 ± 0.1	75.6 ± 0.3	75.3 ± 0.2
PLA	59.4 ± 0.4	85.2 ± 0.3	105.2 ± 0.2	170.3 ± 0.3	29.1 ± 0.2	38.4 ± 0.1
PLA/2CNF	63.2 ± 0.4	85.6 ± 0.5	114.1 ± 0.3	170.4 ± 0.4	29.4 ± 0.4	45.4 ± 0.1
PLA/4PEG	58.7 ± 0.7	75.9 ± 0.1	114.8 ± 0.2	170.1 ± 0.2	34.2 ± 0.1	49.1 ± 0.1
PLA/2CNF/4PEG	58.6 ± 0.6	76.1 ± 0.1	124.1 ± 0.2	169.9 ± 0.1	32.0 ± 0.1	51.0 ± 0.1

All temperatures indicate the values at the corresponding peak; PEG-contained samples showed single peaks for melting and crystallization

<sup>a</sup> The  $T_g$  data have been extracted from the DMTA tests

and CNFs on the crystallization of PLA. PEG could play two roles: first it acts as a plasticizer and, second, it helps the dispersion/distribution of CNFs. On the other hand, nanofibers can have a nucleating effect on the crystallization of the plasticized PLA. Similar synergistic effects of plasticization and nucleation have been reported for PLA/talc/PEG composites (Wang et al. 2010; Courgneau et al. 2013). Contrary to our results, Lee et al. (2012) reported a decrease in the crystallization temperature of PLA in presence of 5 wt% BCNFs and 4.75 wt% copolymer. The values of  $T_{cc}$  and  $T_m$  for the composite sample without PEG are similar to those of PLA. However,  $T_{cc}$  of PLA decreases by 9 °C for PEG-contained samples; this fact supports the idea that PEG acts as a plasticizer.

### Tensile properties

Figure 7 presents normalized values of the Young modulus, tensile strength, and elongation at break for the solution- and melt-prepared samples. The Young modulus of PLA increases for solution-prepared samples containing either CNFs or PEG-compatible CNFs (Fig. 7a). In all cases, the incorporation of nanofibers enhances the Young modulus due to their reinforcing role. Indeed, as the first heating sequence crystallinity of the samples containing 2 wt% CNFs with and without PEG is lower than that of the PLA/4PEG or the same as that of the PLA, respectively (Table 2), the reinforcing role of nanofibers is the dominant factor that improves the modulus rather than the nucleating/crystallization effect. In other words, when the crystalline content of PLA/4PEG decreases in presence of the nanofibers and this may lead to a lower modulus, the presence of a strong CNF network in the PLA/2CNF/4PEG compensates that effect. The tensile strength shows almost the same trend (Fig. 7b). It is interesting to note that other investigators have reported lower enhancements for the Young modulus and tensile strength of PLA/CNF composites with a similar or larger CNF contents, although compatibilization and/or CNF modification were employed (Mathew et al. 2006; Wang and Sain 2007; Qu et al. 2010; Lee et al. 2012). As expected, the elongation at break decreases in the presence of nanofibers (Fig. 7c) as is the case for many composite systems. Figure 7 also depicts no property

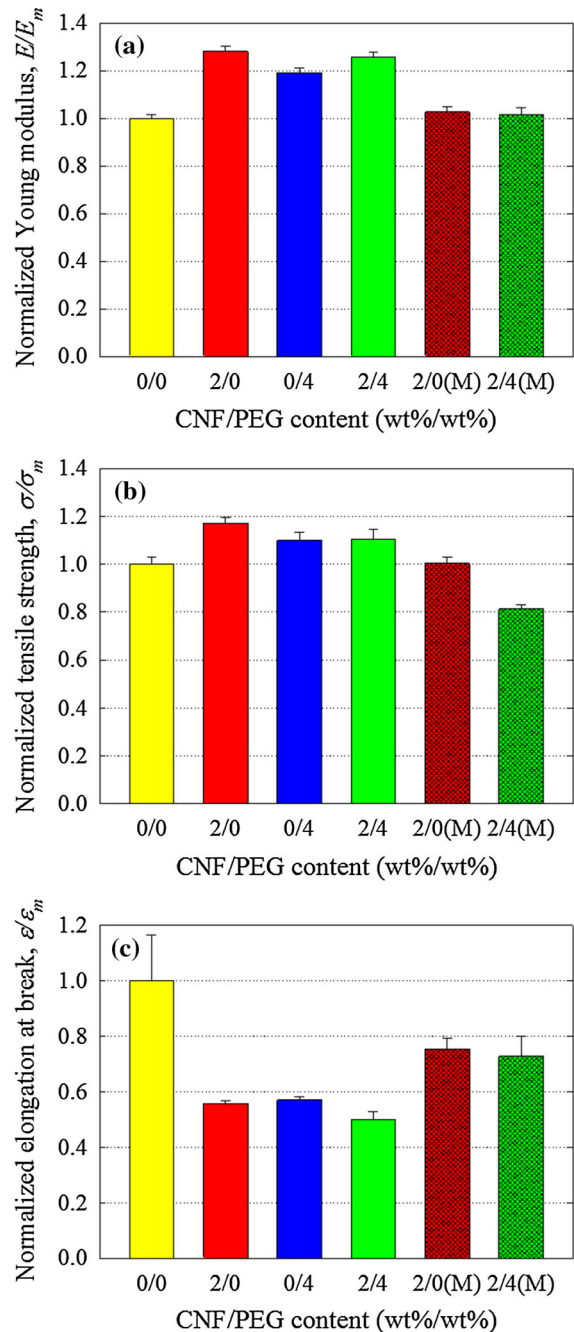


**Fig. 7** Normalized values of tensile properties: **a** Young's modulus, **b** tensile strength and **c** elongation at break for the samples prepared in the solution and molten states. Subscript  $m$  refers to the PLA with Young's modulus, tensile strength and elongation at break of 2.96 GPa, 66.3 MPa and 4%, respectively



enhancement for the melt-based composites relative to the neat PLA as the nanofibers are probably poorly dispersed/distributed in the samples.

## DMTA

Figure 8 presents the flexural storage modulus,  $E'$ , and  $\tan \delta$  for the samples prepared in solution as functions of temperature. The storage modulus of PLA increases over a wide range of temperatures by incorporating the nanofibers; the largest increases are observed in the rubbery region when CNFs are added to the PLA via the masterbatch (Fig. 8a). In fact, a good dispersion and strong entangled network of the nanofibers within the matrix can make the material stiffer (Azizi Samir et al. 2004; Jonoobi et al. 2010; Safdari et al. 2016b, c). The  $\tan \delta$  peak (Fig. 8b), which is taken as the glass transition temperature,  $T_g$ , is reported in Table 2 for the different samples.  $T_g$  of PLA is not affected significantly by the addition of the CNFs, compatibilizer nor the masterbatch; it increases from 59 to 63 °C for PLA and PLA/2CNF, respectively. However, with the incorporation of either the CNFs or the compatibilizer within the PLA phase, the area under the  $\tan \delta$  peak of PLA decreases. In the case where a masterbatch has been used to prepare the final composite, i.e., PLA/2CNF/4PEG, this reduction is more significant. The normalized area,  $A/A_m$  (where subscript  $m$  refers to the PLA), under the  $\tan \delta$  peaks of PLA/2CNF and PLA/2CNF/4PEG decreases to 0.66 and 0.51, respectively. This indicates restricted PLA chain motion as a result of the good dispersion of the CNFs creating a large interfacial area (Bagheriasl et al. 2015; Safdari

et al. 2016b, c) and the effect of PEG on the crystallinity of PLA (see Table 2).

Figure 9 compares the normalized flexural storage modulus,  $E'/E'_m$ , at 25 and 80 °C. The storage modulus of PLA at 25 °C (1.71 GPa) increases up to 42% for PLA/2CNF/4PEG (Fig. 9a). Moreover, in the rubbery region, 132 and 553% enhancement in the storage modulus of PLA (3.9 MPa at 80 °C) is achieved for the samples containing 2 wt% CNFs without and with PEG, respectively (Fig. 9b). This shows that the reinforcement of the nanofibers is more effective when the matrix has a lower modulus in the rubbery region (Suryanegara et al. 2009), and also confirms that a good state of dispersion is achieved using the compatibilizer; thus, PLA products can be exposed to higher temperatures.

## Optical properties

Good dispersion/distribution of nanoparticles in the composite does not usually deteriorate the original transparency of the matrix (Pettersson and Oksman 2006; Eichhorn et al. 2010; Safdari et al. 2016b, c), which could be beneficial for many applications. Figure 10 shows the transmittance for PLA, PLA/2CNF and PLA/2CNF/4PEG films as a function of wavelength,  $\lambda$ . In the visible light range, i.e.,  $\lambda = 390\text{--}700$  nm, the light transparency of PLA does not change significantly due to the presence of the nanofibers. Furthermore, the PLA/2CNF/4PEG film shows even smaller deviations from the transmittance values of the neat PLA film compared to the PLA/2CNF film, even though the crystalline content and the

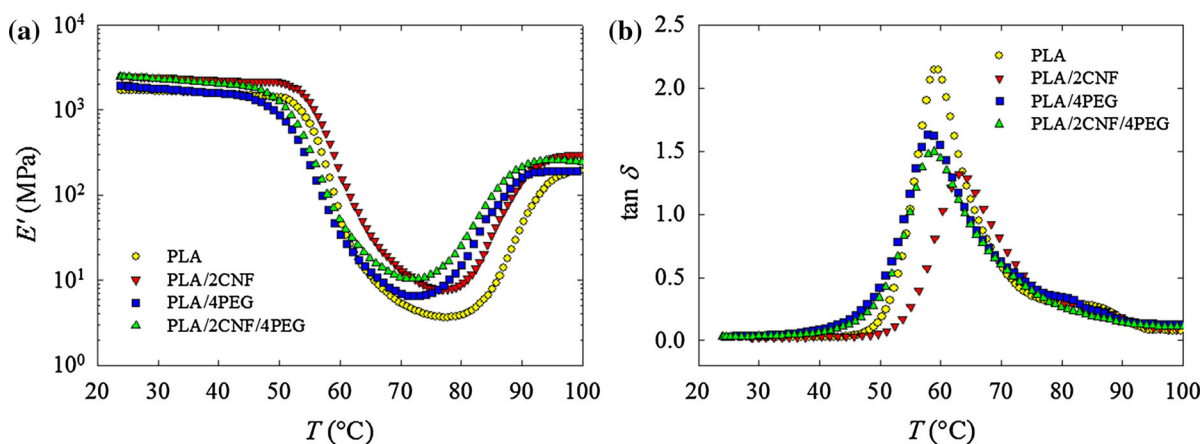


**Fig. 8** **a** Flexural storage modulus and **b**  $\tan \delta$  of the solution-prepared samples

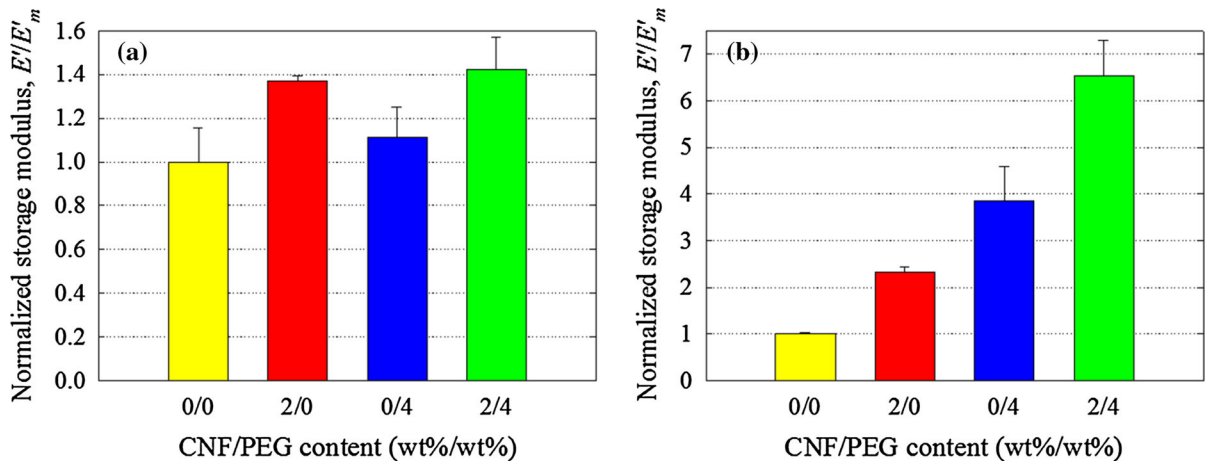


**Fig. 9** Normalized flexural storage modulus at **a** 25 °C and **b** 80 °C for samples prepared in the solution state

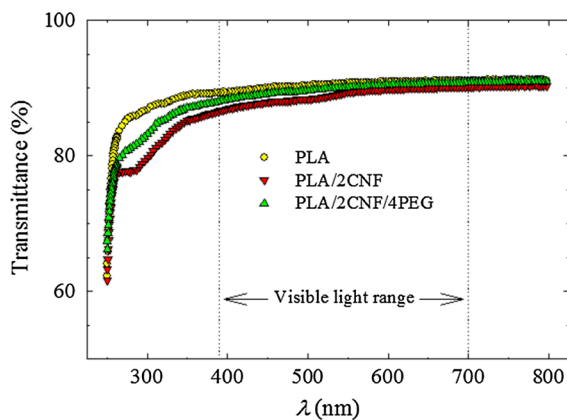


**Fig. 10** Light transmittance of PLA, PLA/2CNF and PLA/2CNF/4PEG films

ratio of CNFs to PLA are slightly larger in the former. This confirms that in the presence of PEG the CNFs are better dispersed/distributed in PLA (Pettersson and Oksman 2006; Safdari et al. 2016b). Nevertheless, both composites show adequate transparency characteristics, since optical transmittance greater than 75% is considered as acceptable transparency for films (Ambrosio-Martín et al. 2015; Safdari et al. 2016b, c). Therefore, these materials can be of interests for optical (Janardhnan and Sain 2011; Xu et al. 2013; Kalia et al. 2014) and optoelectronic (Siró and Plackett 2010; Kalia et al. 2014; Tercjak et al. 2015) applications, whereas it is not the case for composites containing other nano-reinforcements such as carbon nanotubes (Xu et al. 2013). Lower levels of transparency for CNF-filled composites have been reported

where CNFs were poorly dispersed/distributed in the matrix, as translucent films and films with visible agglomerates were seen in some investigations (Jonoobi et al. 2010; Tingaut et al. 2010).

### Concluding remarks

Simple methods were utilized to prepare a CNF/PEG masterbatch and nanofiber-reinforced PLA composites in order to investigate the effects of PEG on the morphology, rheological, thermal, mechanical, and optical properties of PLA/CNF composites. The results of SEM, TEM and AFM indicated a more uniform dispersion/distribution of the nanofibers in the matrix when the CNFs were initially dispersed in PEG prior to mixing with PLA via a solution method. Moreover, a two-phase system was not observed suggesting that PEG and PLA were miscible. Incorporation of CNFs caused substantial increases in the complex viscosity and the storage and loss moduli of PLA for the samples prepared in the solution state; an apparent yield stress was also observed. However, the effect of CNFs on the rheological properties of PLA was more pronounced upon employing the masterbatch method. Increases of one order of magnitude in the complex viscosity, storage and loss moduli for PLA/2CNF/4PEG were observed over the other composite (PLA/2CNF), suggesting better dispersion and distribution of CNFs in this case. The composites prepared using melt processing show much lower increases in rheological properties of the matrix. This

confirms that dispersing highly-entangled CNFs in a matrix via direct mixing in the melt is very challenging, even if a well-dispersed/distributed masterbatch has been already prepared.

The  $T_c$  of PLA shifted up to 19 °C and  $X_c^{cooling}$  of PLA increased by 33% for the compatibilized composite, i.e., PLA/2CNF/4PEG. The storage modulus in DMTA was significantly enhanced for the composites in comparison with the PLA over a wide range of temperatures, especially in the rubbery zone; the storage modulus of PLA at 80 °C was improved by 132 and 553% for the samples containing 2 wt% CNFs without and with PEG, respectively. In the limit of visible light, similar transparencies were observed for both composite films compared to the neat PLA, especially for the composites prepared via the masterbatch.

The results of this study point out to the efficiency of the solution preparation method and the substantial potential of PEG to further increase the properties of PLA/CNF biocomposites. This would promote the use of PLA in applications where its low heat resistance and slow crystallization are serious drawbacks (e.g. film blowing, blow molding and pipes and products exposed to high temperatures); also good optical properties of PLA/CNF films are of interest for optical and optoelectronic applications.

**Acknowledgments** This work was supported by the Natural Sciences and Engineering Research Council of Canada (NSERC) through the Network for Innovative Plastic Materials and Manufacturing Processes (NIPMMP). The authors also wish to thank Professor Mohini M. Sain of the University of Toronto for providing the CNFs.

## References

- Abbasi S, Carreau PJ, Derdouri A, Moan M (2009) Rheological properties and percolation in suspensions of multiwalled carbon nanotubes in polycarbonate. *Rheol Acta* 48:943–959. doi:10.1007/s00397-009-0375-7
- Abdulkhani A, Hosseinzadeh J, Ashori A, Dadashi S, Takzare Z (2014) Preparation and characterization of modified cellulose nanofibers reinforced polylactic acid nanocomposite. *Polym Test* 35:73–79. doi:10.1016/j.polymertesting.2014.03.002
- Adamska K, Voelkel A, Berlińska A (2016) The solubility parameter for biomedical polymers-application of inverse gas chromatography. *J Pharm Biomed Anal* 127:202–206. doi:10.1016/j.jpba.2016.04.014
- Adeosun SO, Lawal GI, Balogun SA, Akpan EI (2012) Review of green polymer nanocomposites. *J Miner Mater Charact Eng* 11:385–416. doi:10.4236/jmmce.2012.114028
- Ambrosio-Martín J, Fabra MJ, Lopez-Rubio A, Lagaron JM (2015) Melt polycondensation to improve the dispersion of bacterial cellulose into polylactide via melt compounding: enhanced barrier and mechanical properties. *Cellulose* 22:1201–1226. doi:10.1007/s10570-014-0523-9
- Arias A, Heuzey MC, Huneault MA, Ausias G, Bendahou A (2015) Enhanced dispersion of cellulose nanocrystals in melt-processed polylactide-based nanocomposites. *Cellulose* 22:483–498. doi:10.1007/s10570-014-0476-z
- Azizi Samir MAS, Alloin F, Paillet M, Dufresne A (2004) Tangling effect in fibrillated cellulose reinforced nanocomposites. *Macromolecules* 37:4313–4316. doi:10.1021/ma035939u
- Azizi Samir MAS, Alloin F, Dufresne A (2005) Review of recent research into cellulosic whiskers, their properties and their application in nanocomposite field. *Biomacromol* 6:612–626. doi:10.1021/bm0493685
- Bagheriasl D, Carreau PJ, Dubois C, Riedl B (2015) Properties of polypropylene and polypropylene/poly(ethylene-co-vinyl alcohol) blend/CNC nanocomposites. *Compos Sci Technol* 117:357–363. doi:10.1016/j.compscitech.2015.07.012
- Bagheriasl D, Carreau PJ, Riedl B, Dubois C (2016a) Enhanced properties of polylactide by incorporating cellulose nanocrystals. *Polym Compos*. doi:10.1002/pc.24259
- Bagheriasl D, Carreau PJ, Riedl B, Dubois C, Hamad WY (2016b) Shear rheology of polylactide (PLA)–cellulose nanocrystal (CNC) nanocomposites. *Cellulose* 23:1885–1897. doi:10.1007/s10570-016-0914-1
- Baiardo M, Frisoni G, Scandola M, Rimelen M, Lips D, Ruffieux K, Wintermantel E (2003) Thermal and mechanical properties of plasticized poly(L-lactic acid). *J Appl Polym Sci* 90:1731–1738. doi:10.1002/app.12549
- Brown EE, Laborie MPG (2007) Bioengineering bacterial cellulose/poly(ethylene oxide) nanocomposites. *Biomacromol* 8:3074–3081. doi:10.1021/bm700448x
- Buddhiranon S, Kim N, Kyu T (2011) Morphology development in relation to the ternary phase diagram of biodegradable PDLA/PCL/PEO blends. *Macromol Chem Phys* 212:1379–1391. doi:10.1002/macp.201100042
- Courgneau C, Ducruet V, Avérous L, Grenet J, Domének S (2013) Nonisothermal crystallization kinetics of poly(lactide)—effect of plasticizers and nucleating agent. *Polym Eng Sci* 53:1085–1098. doi:10.1002/pen.23357
- Eichhorn SJ, Dufresne A, Aranguren M, Marcovich NE, Capadona JR, Rowan SJ, Weder C, Thielemans W, Roman M, Renneckar S, Gindl W, Veigel S, Keckes J, Yano H, Abe K, Nogi M, Nakagaito AN, Mangalam A, Simonsen J, Benight AS, Bismarck A, Berglund LA, Peijs T (2010) Review: current international research into cellulose nanofibres and nanocomposites. *J Mater Sci* 45:1–33. doi:10.1007/s10853-009-3874-0
- Frone AN, Berlioz S, Chailan JF, Panaitescu DM, Donescu D (2011) Cellulose fiber-reinforced polylactic acid. *Polym Compos* 32:976–985. doi:10.1002/pc.21116
- Frone AN, Berlioz S, Chailan JF, Panaitescu DM (2013) Morphology and thermal properties of PLA-cellulose nanofibers composites. *Carbohydr Polym* 91:377–384. doi:10.1016/j.carbpol.2012.08.054
- Ghanbari A, Heuzey MC, Carreau PJ, Ton-That MT (2013a) Morphological and rheological properties of PET/clay

- nanocomposites. *Rheol Acta* 52:59–74. doi:[10.1007/s00397-012-0667-1](https://doi.org/10.1007/s00397-012-0667-1)
- Ghanbari A, Heuzey MC, Carreau PJ, Ton-That MT (2013b) A novel approach to control thermal degradation of PET/organoclay nanocomposites and improve clay exfoliation. *Polymer* 54:1361–1369. doi:[10.1016/j.polymer.2012.12.066](https://doi.org/10.1016/j.polymer.2012.12.066)
- Hendrick E, Frey M (2014) Increasing surface hydrophilicity in poly(lactic acid) electrospun fibers by addition of PLA-b-PEG co-polymers. *J Eng Fibers Fabr* 9:153–164
- Iwatake A, Nogi M, Yano H (2008) Cellulose nanofiber-reinforced polylactic acid. *Compos Sci Technol* 68:2103–2106. doi:[10.1016/j.compscitech.2008.03.006](https://doi.org/10.1016/j.compscitech.2008.03.006)
- Janardhnan S, Sain M (2011) Bio-treatment of natural fibers in isolation of cellulose nanofibres: impact of pre-refining of fibers on bio-treatment efficiency and nanofiber yield. *J Polym Environ* 19:615–621. doi:[10.1007/s10924-011-0312-6](https://doi.org/10.1007/s10924-011-0312-6)
- Jonoobi M, Harun J, Mathew AP, Oksman K (2010) Mechanical properties of cellulose nanofiber (CNF) reinforced polylactic acid (PLA) prepared by twin screw extrusion. *Compos Sci Technol* 70:1742–1747. doi:[10.1016/j.compscitech.2010.07.005](https://doi.org/10.1016/j.compscitech.2010.07.005)
- Jonoobi M, Mathew AP, Abdi MM, Makinejad MD, Oksman K (2012) A comparison of modified and unmodified cellulose nanofiber reinforced polylactic acid (PLA) prepared by twin screw extrusion. *J Polym Environ* 20:991–997. doi:[10.1007/s10924-012-0503-9](https://doi.org/10.1007/s10924-012-0503-9)
- Kalia S, Boufi S, Celli A, Kango S (2014) Nanofibrillated cellulose: surface modification and potential applications. *Colloid Polym Sci* 292:5–31. doi:[10.1007/s00396-013-3112-9](https://doi.org/10.1007/s00396-013-3112-9)
- Kamal MR, Khoshkava V (2015) Effect of cellulose nanocrystals (CNC) on rheological and mechanical properties and crystallization behavior of PLA/CNC nanocomposites. *Carbohydr Polym* 123:105–114. doi:[10.1016/j.carbpol.2015.01.012](https://doi.org/10.1016/j.carbpol.2015.01.012)
- Khoshkava V, Kamal MR (2014) Effect of cellulose nanocrystals (CNC) particle morphology on dispersion and rheological and mechanical properties of polypropylene/CNC nanocomposites. *ACS Appl Mater Interfaces* 6:8146–8157. doi:[10.1021/am500577e](https://doi.org/10.1021/am500577e)
- Kowalczyk M, Piorkowska E, Kulpinski P, Pracella M (2011) Mechanical and thermal properties of PLA composites with cellulose nanofibers and standard size fibers. *Compos Part A Appl Sci Manuf* 42:1509–1514. doi:[10.1016/j.compositesa.2011.07.003](https://doi.org/10.1016/j.compositesa.2011.07.003)
- La Mantia FP, Morreale M (2011) Green composites: a brief review. *Compos Part A Appl Sci Manuf* 42:579–588. doi:[10.1016/j.compositesa.2011.01.017](https://doi.org/10.1016/j.compositesa.2011.01.017)
- Lee KY, Blaker JJ, Bismarck A (2009) Surface functionalisation of bacterial cellulose as the route to produce green polylactide nanocomposites with improved properties. *Compos Sci Technol* 69:2724–2733. doi:[10.1016/j.compscitech.2009.08.016](https://doi.org/10.1016/j.compscitech.2009.08.016)
- Lee KY, Tang M, Williams CK, Bismarck A (2012) Carbohydrate derived copoly(lactide) as the compatibilizer for bacterial cellulose reinforced polylactide nanocomposites. *Compos Sci Technol* 72:1646–1650. doi:[10.1016/j.compscitech.2012.07.003](https://doi.org/10.1016/j.compscitech.2012.07.003)
- Li ZQ, Zhou XD, Pei CH (2010) Preparation and characterization of bacterial cellulose/polylactide nanocomposites. *Polym Plast Technol* 49:141–146. doi:[10.1080/03602550903284198](https://doi.org/10.1080/03602550903284198)
- Lu T, Liu S, Jiang M, Xu X, Wang Y, Wang Z, Gou J, Hui D, Zhou Z (2014) Effects of modifications of bamboo cellulose fibers on the improved mechanical properties of cellulose reinforced poly(lactic acid) composites. *Compos Part B Eng* 62:191–197. doi:[10.1016/j.compositesb.2014.02.030](https://doi.org/10.1016/j.compositesb.2014.02.030)
- Marais A, Kochumalayil JJ, Nilsson C, Fogelström L, Gamstedt EK (2012) Toward an alternative compatibilizer for PLA/cellulose composites: grafting of xyloglucan with PLA. *Carbohydr Polym* 89:1038–1043. doi:[10.1016/j.carbpol.2012.03.051](https://doi.org/10.1016/j.carbpol.2012.03.051)
- Mathew AP, Chakraborty A, Oksman K, Sain M (2006) The structure and mechanical properties of cellulose nanocomposites prepared by twin screw extrusion. In: Oksman K, Sain M (eds) *Cellulose nanocomposites: processing, characterization, and properties*, vol 938. Oxford University Press, Oxford, pp 114–131. doi:[10.1021/bk-2006-0938.ch009](https://doi.org/10.1021/bk-2006-0938.ch009)
- Miao C, Hamad WY (2013) Cellulose reinforced polymer composites and nanocomposites: a critical review. *Cellulose* 20:2221–2262. doi:[10.1007/s10570-013-0007-3](https://doi.org/10.1007/s10570-013-0007-3)
- Nakagaito AN, Fujimura A, Sakai T, Hama Y, Yano H (2009) Production of microfibrillated cellulose (MFC)-reinforced polylactic acid (PLA) nanocomposites from sheets obtained by a papermaking-like process. *Compos Sci Technol* 69:1293–1297. doi:[10.1016/j.compscitech.2009.03.004](https://doi.org/10.1016/j.compscitech.2009.03.004)
- Petersson L, Oksman K (2006) Biopolymer based nanocomposites: comparing layered silicates and microcrystalline cellulose as nanoreinforcement. *Compos Sci Technol* 66:2187–2196. doi:[10.1016/j.compscitech.2005.12.010](https://doi.org/10.1016/j.compscitech.2005.12.010)
- Plummer CG, Choo CC, Boissard CR, Bourban PE, Månson JA (2013) Morphological investigation of polylactide/microfibrillated cellulose composites. *Colloid Polym Sci* 291:2203–2211. doi:[10.1007/s00396-013-2968-z](https://doi.org/10.1007/s00396-013-2968-z)
- Qu P, Gao Y, Wu G, Zhang L (2010) Nanocomposites of poly(lactic acid) reinforced with cellulose nanofibrils. *BioResources* 5:1811–1823
- Ramezani Kakroodi A, Cheng S, Sain M, Asiri A (2014) Mechanical, thermal, and morphological properties of nanocomposites based on polyvinyl alcohol and cellulose nanofiber from aloe vera rind. *J Nanomater* 2014:1–7. doi:[10.1155/2014/903498](https://doi.org/10.1155/2014/903498)
- Raquez JM, Habibi Y, Murariu M, Dubois P (2013) Polylactide (PLA)-based nanocomposites. *Prog Polym Sci* 38:1504–1542. doi:[10.1016/j.progpolymsci.2013.05.014](https://doi.org/10.1016/j.progpolymsci.2013.05.014)
- Safdari F, Bagheriasl D, Carreau PJ, Heuzey MC, Kamal MR (2016a) High-performance polylactide biocomposites reinforced with cellulose nanofibers. *SPE Plast Res*. doi:[10.2417/spepro.006650](https://doi.org/10.2417/spepro.006650)
- Safdari F, Bagheriasl D, Carreau PJ, Heuzey MC, Kamal MR (2016b) Rheological, mechanical, and thermal properties of polylactide/cellulose nanofiber biocomposites. *Polym Compos*. doi:[10.1002/pc.24127](https://doi.org/10.1002/pc.24127)
- Safdari F, Carreau PJ, Heuzey MC, Kamal MR, Sain MM (2016c) Enhanced properties of poly(ethylene



- oxide)/cellulose nanofiber biocomposites. *Cellulose*. doi:[10.1007/s10570-016-1137-1](https://doi.org/10.1007/s10570-016-1137-1)
- Saffar A, Jalali Dil E, Carreau PJ, Ajji A, Kamal MR (2016) Phase behavior of binary blends of PP/PP-g-AA: limitations of the conventional characterization techniques. *Polym Int* 65:508–515. doi:[10.1002/pi.5082](https://doi.org/10.1002/pi.5082)
- Sanchez-Garcia M, Lagaron J (2010) On the use of plant cellulose nanowhiskers to enhance the barrier properties of polylactic acid. *Cellulose* 17:987–1004. doi:[10.1007/s10570-010-9430-x](https://doi.org/10.1007/s10570-010-9430-x)
- Sheth M, Kumar RA, Davé V, Gross RA, McCarthy SP (1997) Biodegradable polymer blends of poly(lactic acid) and poly(ethylene glycol). *J Appl Polym Sci* 66:1495–1505. doi:[10.1002/\(SICI\)1097-4628\(19971121\)66:8<1495:AID-APP10>3.0.CO;2-3](https://doi.org/10.1002/(SICI)1097-4628(19971121)66:8<1495:AID-APP10>3.0.CO;2-3)
- Siró I, Plackett D (2010) Microfibrillated cellulose and new nanocomposite materials: a review. *Cellulose* 17:459–494. doi:[10.1007/s10570-010-9405-y](https://doi.org/10.1007/s10570-010-9405-y)
- Suryanegara L, Nakagaito AN, Yano H (2009) The effect of crystallization of PLA on the thermal and mechanical properties of microfibrillated cellulose-reinforced PLA composites. *Compos Sci Technol* 69:1187–1192. doi:[10.1016/j.compscitech.2009.02.022](https://doi.org/10.1016/j.compscitech.2009.02.022)
- Tercjak A, Gutierrez J, Barud HS, Domenegueti RR, Ribeiro SJL (2015) Nano- and macroscale structural and mechanical properties of in situ synthesized bacterial cellulose/PEO-b-PPO-b-PEO biocomposites. *ACS Appl Mater Interfaces* 7:4142–4150. doi:[10.1021/am508273x](https://doi.org/10.1021/am508273x)
- Tingaut P, Zimmermann T, Lopez-Suevos F (2010) Synthesis and characterization of bionanocomposites with tunable properties from poly(lactic acid) and acetylated microfibrillated cellulose. *Biomacromol* 11:454–464. doi:[10.1021/bm901186u](https://doi.org/10.1021/bm901186u)
- Tome LC, Pinto RJB, Trovatti E, Freire CSR, Silvestre AJD, Neto CP, Gandini A (2011) Transparent bionanocomposites with improved properties prepared from acetylated bacterial cellulose and poly(lactic acid) through a simple approach. *Green Chem* 13:419–427. doi:[10.1039/COGC00545B](https://doi.org/10.1039/COGC00545B)
- Wang T, Drzal LT (2012) Cellulose-nanofiber-reinforced poly(lactic acid) composites prepared by a water-based approach. *ACS Appl Mater Interfaces* 4:5079–5085. doi:[10.1021/am301438g](https://doi.org/10.1021/am301438g)
- Wang B, Sain M (2007) The effect of chemically coated nanofiber reinforcement on biopolymer based nanocomposites. *BioResources* 2:371–388
- Wang Y, Li M, Hu D, Shen C (2010) Accelerating the crystallization of poly(lactic acid). *SPE Plast Res*. doi:[10.1002/spepro.002983](https://doi.org/10.1002/spepro.002983)
- Wu CS (2009) Renewable resource-based composites of recycled natural fibers and maleated polylactide bioplastic: characterization and biodegradability. *Polym Degrad Stab* 94:1076–1084. doi:[10.1016/j.polydegradstab.2009.04.002](https://doi.org/10.1016/j.polydegradstab.2009.04.002)
- Xu X, Liu F, Jiang L, Zhu JY, Haagensohn D, Wiesenborn DP (2013) Cellulose nanocrystals vs. cellulose nanofibrils: a comparative study on their microstructures and effects as polymer reinforcing agents. *ACS Appl Mater Interfaces* 5:2999–3009. doi:[10.1021/am302624t](https://doi.org/10.1021/am302624t)
- Xu X, Wang H, Jiang L, Wang X, Payne SA, Zhu JY, Li R (2014) Comparison between cellulose nanocrystal and cellulose nanofibril reinforced poly(ethylene oxide) nanofibers and their novel shish-kebab-like crystalline structures. *Macromolecules* 47:3409–3416. doi:[10.1021/ma402627j](https://doi.org/10.1021/ma402627j)
- Zhang K, Nagarajan V, Misra M, Mohanty AK (2014) Super-toughened renewable PLA reactive multiphase blends system: phase morphology and performance. *ACS Appl Mater Interfaces* 6:12436–12448. doi:[10.1021/am502337u](https://doi.org/10.1021/am502337u)
- Zhou C, Shi Q, Guo W, Terrell L, Qureshi AT, Hayes DJ, Wu Q (2013) Electrospun bio-nanocomposite scaffolds for bone tissue engineering by cellulose nanocrystals reinforcing maleic anhydride grafted PLA. *ACS Appl Mater Interfaces* 5:3847–3854. doi:[10.1021/am4005072](https://doi.org/10.1021/am4005072)